Zuschriften
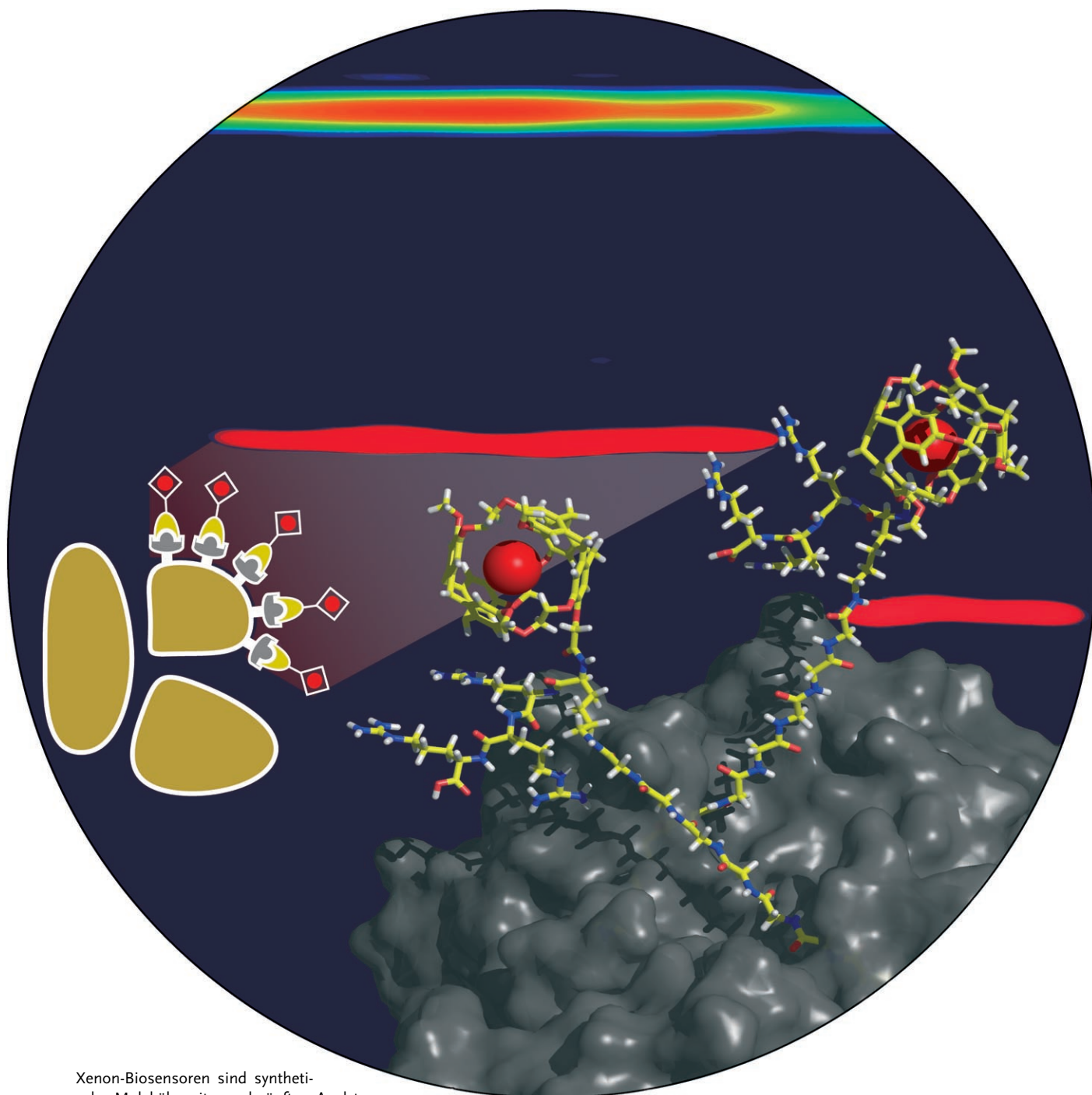
Xenon-Biosensoren sind synthetische Moleküle mit angeknüpften Analyt und Xenon bindenden Einheiten. Die Assoziation mit dem Analyt führt zu ungewöhnlichen NMR-Signalen, wobei die Empfindlichkeit durch hyperpolarisiertes Xenon stark erhöht wird. Einzelheiten zur Anwendung von Xenon-Biosensoren in der biomedizinischen Bildgebung besprechen C. Hilty et al. in der Zuschrift auf den folgenden Seiten.

# Spectrally Resolved Magnetic Resonance Imaging of a Xenon Biosensor**

Christian Hilty,* Thomas J. Lowery, David E. Wemmer, and Alexander Pines

Nuclear magnetic resonance is the method of choice for applications as widespread as chemical analysis and medical diagnostics because of its ability to non-invasively record images, as well as elucidate molecular structure. Its detection threshold is, however, limited by the small polarization of nuclear spins in even the highest available magnetic fields. This limitation can, under certain circumstances, be alleviated by using hyperpolarized substances.[1] Xenon biosensors make use of the sensitivity gain obtained with hyperpolarized xenon to provide the capability for magnetic resonance detection of a specific low-concentration target.[2–4] Such biosensors consist of a cryptophane cage[5] which binds one xenon atom, and is connected through a linker to a targeting moiety such as a ligand or antibody (Figure 1). Recent work has shown the possibility of using the xenon biosensor to detect small amounts of a substance in a heterogeneous environment by NMR spectroscopy.[6] Here, we demonstrate that magnetic resonance (MR) provides the capability of obtaining spectrally and spatially resolved images of the distribution of the immobilized biosensor, thus opening up the possibility of using the xenon biosensor for targeted imaging.

A continuous flow of water saturated with hyperpolarized xenon was supplied by a specifically designed apparatus (Figure 2) to immobilized avidin–agarose beads (ca. 250 μL hydrated volume) packed in a glass tube assembly between two frits (Figure 3a). The xenon biosensor was attached to the
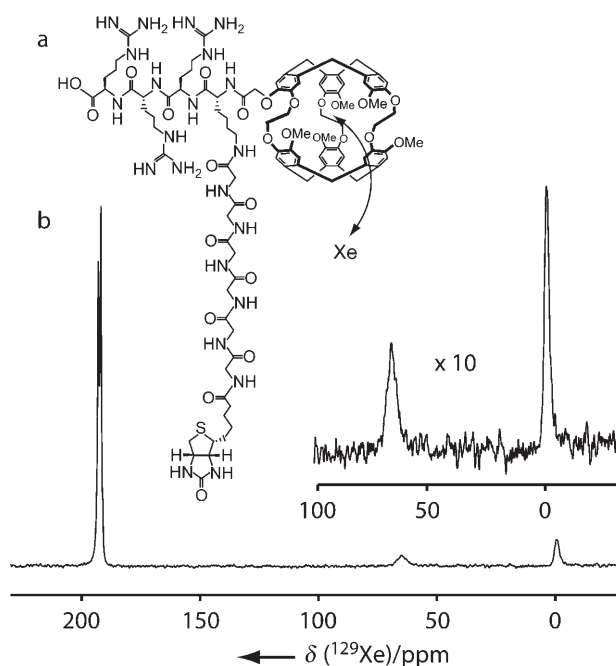
Figure 1. a) Chemical structure of the functionalized xenon biosensor.[2, 6] b) NMR spectrum of the xenon biosensor bound to avidin-containing agarose beads.
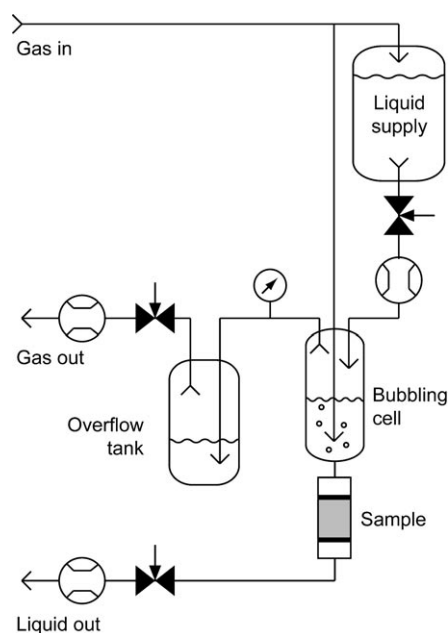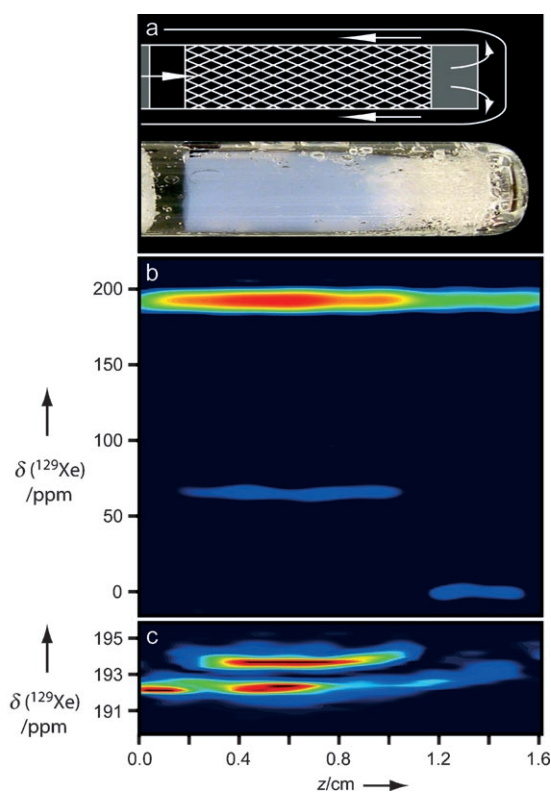

Figure 2. Instrumentation for MR imaging with xenon-saturated liquids.

[*] Dr. C. Hilty, Prof. A. Pines
Lawrence Berkeley National Laboratory
Materials Sciences Division
and
University of California Berkeley
Department of Chemistry
Berkeley CA 94720 (USA)
Fax: (+1) 510-486-5744
E-mail: hilty@berkeley.edu

T. J. Lowery, Prof. D. E. Wemmer
Lawrence Berkeley National Laboratory
Physical Biosciences Division
and
University of California Berkeley
Department of Chemistry
Berkeley CA 94720 (USA)

agarose beads through the affinity of its biotin tag to immobilized avidin (binding affinity: $10^{15}\,\text{M}^{-1}$). It was estimated from biochemical characterization that a biosensor concentration of 82 μM was thus achieved in the resin. The biosensor construct used is shown in Figure 1, with its xenon-binding cryptophane cage to the right and its biotin tag at the bottom.

Figure 3. a) Sketch and photograph of the agarose bead sample used for the imaging experiments. The direction of liquid flow (indicated by arrows) is from left to right, through the column of beads (hatched), out the frit (shaded gray), and around the outside of the inner concentric tube. b) Spectrally resolved MR image of the immobilized xenon biosensor. The image dimension (horizontal) is shown to scale with the photograph in (a). The image was taken over 135 minutes, using a field of view along the z-dimension of 2 cm and a resolution of 1.2 mm. c) Image of the solution peak in (b), processed to show splitting between the xenon in the bead and xenon in water.

The signal at $\delta = 65.4$ ppm with a linewidth of 300 Hz in the ^{129}Xe NMR spectrum of this sample (Figure 1) corresponds to xenon in the biosensor. The downfield signals at $\delta = 193.6$ and 192.5 ppm are from dissolved xenon in the agarose beads and water, respectively,[6] and the signal at $\delta = 0$ ppm is from xenon gas. The xenon resonance from the immobilized biosensor is broadened relative to that of the solution-free biosensor (ca. 20 Hz),[2,7] presumably because of motional hindrance of the cage.

A spectrally resolved image of the biosensor distribution in this sample was acquired using phase-encoded MR imaging (Figure 3). Figure 3a shows a photograph of the sample with flowing xenon-saturated water for comparison. Drawn to scale with this photograph is the xenon image that has spatial resolution along the z axis (Figure 3b). It is readily apparent that different regions of the sample give rise to the signals with different chemical shift. The image intensity at the chemical shift of the dissolved xenon ($\delta \approx 193$ ppm) extends over the entire sample space, while the signal at the chemical shift of xenon in the biosensor ($\delta = 65.4$ ppm) occurs only in the actual volume of the beads. To the right of the image, a short section of xenon gas ($\delta = 0$ ppm) is visible, which corresponds to the region in the sample where gas bubbles appear in the photograph (Figure 3a). This gas release is due to a pressure gradient over the column of beads. The spectral dimension in Figure 3b is processed with a sine bell window in which only the first part of the free induction decay (FID) is selected, where the signal corresponding to the biosensor is present. As a consequence, the signal of dissolved xenon is not resolved into its water and bead components in this image. The splitting of this signal becomes readily observable when an exponential window function that extends over the entire FID is applied (Figure 3c). Here, the extent of the bead volume can be deduced from the signal at $\delta = 193.6$ ppm, which closely corresponds to the size of the biosensor signal. The slight change in chemical shift of the solution signals between $z = 1$ to $z = 1.4$ cm may be attributable to susceptibility differences between the agarose beads, gas bubbles, and the lower frit.

These experiments show that MR imaging of a selectively targeted xenon biosensor can be accomplished with good sensitivity. The use of hyperpolarized xenon enables the distribution of a micromolar range concentration of avidin to be imaged in this heterogeneous sample. In comparison, direct detection of bead-bound avidin by ^{1}H NMR spectroscopy would be very difficult or impossible because of the low concentration, broad linewidth, and spectral crowding.

Imaging at the lower NMR coil filling factors required for most in situ samples will demand significant improvements in sensitivity. An increase in the signal by more than a factor of 10 could easily be gained by using a xenon polarizer optimized for continuous flow applications[8] to give a polarization of about 50% instead of 3%. An increase of another factor of 15 could be gained by using a biosensor that does not suffer broadening of the xenon line when immobilized. Further sensitivity could be gained by designing sensor constructs that contain more than one xenon binding cage per analyte, and by the use of isotopically enriched xenon. These improvements would boost the sensitivity of xenon biosensor imaging by a factor of at least 1000. Such an increase extrapolates to a detection threshold of about 100 nM in a small NMR coil optimized for the biosensor-bound sample volume, or to a detection limit of about 100 μM in a sample of the present size in an overall volume of several liters.[9]

From these results, the potential usefulness of a xenon biosensor construct that is targeted to markers on cell surfaces may be extrapolated. In vivo imaging with free hyperpolarized xenon has already been demonstrated.[10,11] In combination with specific targeting, for example, to tumor cells, this could lead to a new tool for medical applications such as the diagnosis of cancer. The xenon biosensor would offer advantages over other methods for the detection of low target concentrations in opaque tissue. In contrast to using hyperpolarized small molecules,[12] the biosensor could be injected well in advance to the introduction of hyperpolarized xenon and acquisition of the signal, thus allowing adequate time for target binding without compromising xenon polarization. As seen in Figure 3b, xenon in the biosensor is easily distinguished from bulk xenon through its different chemical shift. A xenon biosensor image is, therefore, an image with near-zero background, and should afford much higher

detection fidelity than a contrast agent such as gadolinium that merely modulates the proton signal already present in the entire volume.[13] The large chemical shift bandwidth of cage-encapsulated xenon makes the use of the xenon biosensor suitable for multiple analysis, where a number of different biosensors with unique xenon chemical shifts bind to different targets.[2, 4] Our results here indicate that the possibility of multiple biomolecular analysis can be extended to imaging to allow for multiple, target-selective images to be acquired simultaneously (Figure 3), which would greatly enhance the specificity and fidelity of diagnosis.

Experimental Section

An apparatus was designed to provide a continuous stream of liquid saturated with hyperpolarized xenon. Water flowed from the liquid supply (1000 mL) to the bubbling cell (5 mL), where it was saturated with hyperpolarized xenon ($4.4 \, \text{mM} \, \text{atm}^{-1}$;[1, 6] Amersham Health, Durham, NC), then through the sample to the "liquid out" port. The hyperpolarized xenon gas mixture (1% Xe at natural isotope abundance, polarized to ca. 3%, mixed with 10% N_2, 89% He; Airgas, Radnor, PA) was supplied at a pressure of 6 atm to the "gas in" port, and flowed through the bubbling cell to the "gas out" port. The gas also pressurized the liquid supply, so that gravity was sufficient for liquid to flow to the bubbling cell. Both the liquid refill and the sample flow rates were controlled with needle valves and measured with rotameters. To ensure that the bubbling cell did not empty during an experiment, the refill rate was set 50% higher than the flow rate through the sample. The excess water exited the bubbling cell together with the gas and was collected in the overflow tank. The bubbling intensity was controlled by the gas flow rate (0.7 standard liters per minute), which was adjusted at the "gas out" port. The system pressure was monitored at the inlet to the overflow tank.

For the present experiments, the sample of immobilized-avidin, 6% cross-linked, agarose beads (Pierce Biotechnology), with the xenon biosensor was designed to fit within the coil of a 10-mm NMR probe (Varian, Palo Alto, CA), which had a sensitive region of 1.8 cm along the z-axis. The probe was inserted together with a gradient coil assembly into a vertical bore superconducting NMR magnet (7 T). The sample was efficiently perfused by xenon-saturated water, which was refreshed completely every 6 s when using a liquid flow rate of 10 mL min^{-1}. The bubbling cell was located immediately above the sample.

Spectrally resolved MR images were acquired using phase encoding for spatial dimensions and chemical shift resolved acquisition.[14] The pulse sequence was thus $p_{90} - \tau_{\text{grad}} - p_{180} - \tau_{\text{acq}}$. $p_{90} = 14 \, \mu s$ and $p_{180} = 28 \, \mu s$ stand for rf pulses with the indicated flip angle; phase-encoding gradients were applied over $\tau_{\text{grad}} = 200 \, \mu s$; and the spectral dimension was acquired as an echo over $\tau_{\text{acq}} = 100 \, \text{ms}$. The phases of the 90° pulse and the receiver were cycled as $\{x, -x\}$. A delay of 6 s between transients was used.

[1] M. G. Mortuza, S. Anala, G. E. Pavlovskaya, T. J. Dieken, T. Meersmann, *J. Chem. Phys.* **2003**, *118*, 1581–1584.

[2] M. M. Spence, E. J. Ruiz, S. M. Rubin, T. J. Lowery, N. Winssinger, P. G. Schultz, D. E. Wemmer, A. Pines, *J. Am. Chem. Soc.* **2004**, *126*, 15287–15294.

[3] T. J. Lowery, S. M. Rubin, E. J. Ruiz, M. M. Spence, N. Winssinger, P. G. Schultz, A. Pines, D. E. Wemmer, *Magn. Reson. Imaging* **2003**, *21*, 1235–1239.

[4] M. M. Spence, S. M. Rubin, I. E. Dimitrov, E. J. Ruiz, D. E. Wemmer, A. Pines, S. Q. Yao, F. Tian, P. G. Schultz, *Proc. Natl. Acad. Sci. USA* **2001**, *98*, 10654–10657.

[5] A. Collet, *Tetrahedron* **1987**, *43*, 5725–5759.

[6] S. I. Han, S. Garcia, T. J. Lowery, E. J. Ruiz, J. A. Seeley, L. Chavez, D. S. King, D. E. Wemmer, A. Pines, *Anal. Chem.* **2005**, *77*, 4008–4012.

[7] T. J. Lowery, S. Garcia, L. Chavez, E. J. Ruiz, T. Wu, T. Brotin, J.-P. Dutasta, D. S. King, P. G. Schultz, A. Pines, D. E. Wemmer, *ChemBioChem* **2005**, in press.

[8] K. Knagge, J. Prange, D. Raftery, *Chem. Phys. Lett.* **2004**, *397*, 11–16.

[9] D. I. Hoult, *Prog. Nucl. Magn. Reson. Spectrosc.* **1978**, *12*, 41–77.

[10] M. S. Albert, G. D. Cates, B. Driehuys, W. Happer, B. Saam, C. S. Springer, A. Wishnia, *Nature* **1994**, *370*, 199–201.

[11] B. M. Goodson, Y. Q. Song, R. E. Taylor, V. D. Schepkin, K. M. Brennan, G. C. Chingas, T. F. Budinger, G. Navon, A. Pines, *Proc. Natl. Acad. Sci. USA* **1997**, *94*, 14725–14729.

[12] K. Golman, J. H. Ardenaer-Larsen, J. S. Petersson, S. Mansson, I. Leunbach, *Proc. Natl. Acad. Sci. USA* **2003**, *100*, 10435–10439.

[13] M. L. Wood, P. A. Hardy, *Magn. Reson. Imaging* **1993**, *3*, 149–156.

[14] P. T. Callaghan, *Principles of Nuclear Magnetic Resonance Microscopy*, Oxford University Press, New York, **1991**.